Integrated device with diffractive polarization components for a magneto-optical disk head

Charles W. Haggans and Teruo Fujita*
Optical Sciences Center
University of Arizona
Tucson, AZ 85721
(602)-621-2031

Raymond K. Kostuk
Electrical and Computer Engineering Department
and Optical Sciences Center
University of Arizona
Tucson, AZ 85721

1. INTRODUCTION

The optical components in the detection train of a conventional magneto-optical (M-O) disk head include a half-wave plate and a polarization beamsplitter. These polarization components are bulky and require specialized mounting hardware. In order to realize a more compact head, we propose that these elements be replaced by an integrated device composed of cascaded volume and surface-relief gratings. In this paper, we describe the proposed system, detail designs for the individual elements, compare theoretical and prototype element performance, and discuss the operational tolerances of these elements.

Several authors have reported efforts to replace individual conventional elements in the M-O head detection train with diffractive elements.[1-5] The most comprehensive of these studies was that of Ono et. al.[1] in which focus and tracking error signals and the M-O signal were generated using a multifunctional holographic optical element (HOE). However, the angular separation of the transmitted and diffracted beams generated by this element (1°) limits the compactness of the assembled system (assuming a detector spacing of 500 μm, the leaky beamsplitter to detector plane spacing must be approximately 30 mm). Our proposed device is much more compact because all detection train elements are integrated onto two thin substrates. Thus, the leaky beamsplitter to detection plane distance is approximately 8 mm for a 4 mm diameter beam.

2. DEVICE LAYOUT

Figure 1 is a schematic diagram of a conventional M-O head. The detection train is indicated in this figure. We propose to replace the detection train components with a substrate-mode device, giving the system configuration shown in Figure 2. The leaky beamsplitter to detector distance with this device is reduced significantly from the conventional head design (~8 mm as opposed to ~30 mm). The optical path of this device is an integrated version of a detection train design presented by Milster[6] and Matsubayashi.[7] This differs from the conventional detection train in that circularly polarized light is incident on the polarization beamsplitter due to the presence of a quarter-wave retarder.

The proposed device is detailed in Figure 3. The beam incident on the device from the leaky beamsplitter is primarily p polarized (the electric field vector in the plane of the drawing). The beam also contains the small s polarized signal introduced by reflection from the M-O medium as well as any phase difference introduced between the two polarizations due to the M-O medium, the disk substrate, the folding mirror, and the leaky beamsplitter. This beam is coupled into the substrate mode by Element 1. This element is a slanted volume grating fabricated holographically in dichromated gelatin. This grating has a high diffraction efficiency and causes negligible polarization conversion (rotation) or phase shift between the s and p components of the incident beam. After propagating through the substrate, the beam is reflected from a high spatial frequency lamellar (rectangular) grating at the boundary between the glass substrate and a metallic layer. This grating acts as a quarter-wave retarder in that the reflected beam has an s-p phase difference of approximately -90°. Element 3 is a lamellar grating at the top of the substrate that is also formed between the glass and a metallic layer. This grating is oriented so that the polarization angle of the reflected 0th order beam is rotated by 45° with respect to that of the incident beam. Thus, the polarization angle of the beam reflected from this grating is oriented at $45° \pm |\Theta_x|$ with respect to the p polarization component direction. The phase difference between the s and p components of the reflected beam is 90°. This means that the beam reflected from Element 3 is nearly circularly polarized. Finally, a lamellar grating formed between the substrate and air (element 4) acts as a polarization beamsplitter, separating the s and p polarization components for differential signal detection with a high extinction ratio.

Focus and tracking error sensing is implemented on the s and p polarized beams exiting Element 4. The propagation directions of these beams vary with wavelength due to the diffractive nature of elements 1-4. However, a push-pull tracking error signal can be generated from the p polarized beam transmitted by Element 4 by aligning the split detector so that the beam moves along the separation between the detectors as the wavelength varies.

A focus error signal can be generated from the s polarized beam diffracted by Element 4 with an off-axis pupil obscuration method. Figure 3 shows a focus error sensing path consisting of a reflectively coated cylindrical lens, a knife-edge, and a split detector. The separation between the detector halves is parallel to the plane of the paper. In this path, the s polarized beam comes to a line focus that is inclined with respect to the detector plane. When the objective is properly focused on the M-O disk, the signal detected by the left and right detector halves cancels as in the standard pupil obscuration method. For an out of focus disk, the intensity pattern on the detector plane is asymmetric with respect to the split line of the detector. Thus, while the intensity pattern on the split detector is highly aberrated, its symmetry allows for focus error signal generation.

3. COMPONENT AND DEVICE MODELING

The polarization properties of the grating elements composing this device have been calculated using rigorous vector coupled-wave[8,9] and modal[10] grating diffraction models. The modal model has been used for metallic surface-relief grating cases where convergence was not achieved with the coupled-wave model.[11] In this paper, we use the notation of Born and Wolf[12] to describe the state of polarization of the substrate-mode beams. The electric field vector for an elliptically polarized beam can be written as

$$E=\hat{s}A_s\exp(i[\mathbf{k}\cdot\mathbf{r}-\omega t-\phi_s]) + \hat{p}A_p\exp(i[\mathbf{k}\cdot\mathbf{r}-\omega t-\phi_p]). \quad (1)$$

The polarization state of this beam is fully described by the angular ratio of the s and p polarization component amplitudes,

$$\alpha=\mathrm{atan}(A_s/A_p), \quad (2)$$

and the phase difference between the s and p polarization components,

$$\delta=\phi_s-\phi_p. \tag{3}$$

An elliptically polarized beam can also be uniquely described by two other angular parameters: the polarization rotation angle Θ and the ellipticity ε. These parameters can be related to α and δ by

$$\tan 2\Theta = \tan 2\alpha \cos\delta \tag{4}$$

and

$$\sin 2\varepsilon = \sin 2\alpha \sin\delta. \tag{5}$$

The grating and incidence geometries used in this paper are defined in Figure 4. A subscript of i denotes parameters relating to the incident beam and subscripts of r and t denote reflected and transmitted beam parameters, respectively.

The polarization characteristics required for Elements 1-4 are summarized in Sections 3.1-3.4. In each section, grating dimensions and incidence parameters are given for an element designed for operation at a wavelength of 0.780 μm. Finally, in Section 3.5, the integrated performance of these four elements is detailed. For these computations, the propagation angle within the substrate was chosen to be 45° and the substrate refractive index was chosen to be 1.517. For Elements 2 and 3, the metallic external medium was chosen to be gold ($n=0.175$, $\kappa=4.91$).[13]

3.1 Unselective Incoupler

The first element of this device must couple the normally incident beam into the substrate with high efficiency and negligible polarization rotation ($\alpha_t=45°$). The period of this grating (Λ) must be 0.727 μm in order to obtain a propagation angle of 45° in the substrate. We investigated the potential for using a triangular profile (blazed) grating as the first element. However, rigorous modeling indicated that efficiencies greater than 0.5 were not achievable for a surface-relief element in this diffraction geometry. Thus, we propose that a slanted grating fabricated in dichromated gelatin (DCG) be used for this element.

The coupled-wave volume grating model indicates that a DCG grating can theoretically have an efficiency of 0.9 with negligible change to the incident values of α and δ. This is possible for a DCG grating with a period of 0.727 μm, an emulsion thickness of 8.75 μm, a bulk emulsion refractive index of 1.44, and an index modulation of 0.0435.

3.2 Quarter-Wave Retarder

The second element in this device is a metalized lamellar (rectangular) grating. This grating is oriented with the grating vector either parallel or perpendicular to the plane of incidence ($\Phi=0°$ or 90°). We have previously reported[14] that this type of grating can function as a quarter-wave retarder. In this device, this element introduces a -90° s-p phase difference to the incident beam ($\alpha_i=\pm 0.5°$, $\delta_i=0°$) so that the reflected beam is nearly circularly polarized. All diffracted orders other than the specularly reflected order are suppressed upon reflection from this grating because the grating period satisfies the relation

$$\Lambda \le \lambda/[n(\sin\Theta+\sin 90°)], \tag{6}$$

where n is the substrate refractive index and Θ is the propagation angle of the substrate-mode beam with respect to the grating normal. For the parameters chosen for this device, the maximum allowable period for this grating is 0.301 μm.

A lamellar grating coated with gold can introduce the desired phase shift to the incident beam. A grating with d=0.205 μm, Λ=0.3 μm, and dc=0.5 that is oriented with Φ=90° gives δ_t=-90° and α_t=±0.5° for an incident beam with δ_i=0° and α_i=±0.5°. The efficiency for reflection from this grating is 0.92.

3.3 Polarization Rotator

The third element of this device is used for polarization rotation (modification of α_t) to nearly equalize the s and p polarization component amplitudes of the substrate-mode beam. This is done with a half-wave plate in conventional systems to maximize the differentially generated M-O signal. For conical incidence (Φ≠0°) on a lamellar grating at a glass-metal interface, the amount of polarization rotation imparted to the reflected beam can be chosen by varying d and Φ. A grating with Λ=0.3 μm, d=0.155 μm, and dc=0.5 oriented with Φ=44° changes the state of polarization from α_i=±0.5° and δ_i=-90° to α_t=45 ± 0.5° and δ_t=90°. The efficiency of reflection from this grating is 0.90.

3.4 Polarization Beamsplitter

Element 4 is a polarization beamsplitter that separates the components of the incident beam with high efficiency and a high extinction ratio. This is accomplished with a lamellar grating at the boundary between the first and second substrates of the device. These substrates must be assembled so that the grating grooves are filled with air (optical cement or index matching fluid must not fill the grating grooves).

A grating of this type with Λ=0.364 μm, d=0.98 μm, and dc=0.3 oriented with Φ=0° functions as a PBS for this device. The p polarization component is transmitted by this grating without angular deviation with an efficiency of 0.99 and an extinction ratio of 138 ($ER=A_{p,trans}/A_{s,trans}$). The s polarization component is diffracted into the +1st order which lies in a direction that is perpendicular to the p polarized beam. The diffraction efficiency for s polarized light is 0.92 and the extinction ratio is 74.

3.5 Performance of Cascaded Gratings

The previous sections indicate that it is theoretically possible for grating elements to function as the polarization components required in an M-O head detection train. Figure 5 summarizes the calculated properties of the grating elements. The throughput efficiency for elements 1-4 is 0.74 for p polarization and 0.7 for s polarization.

4. EXPERIMENTAL RESULTS

Efforts are underway in our laboratory to fabricate the four diffractive components used in this device. To this point, we have concentrated on fabricating Elements 2 and 3. These elements consist of silver-coated photoresist gratings on soda-lime substrates. These elements have been designed for use at a wavelength of 0.6328 μm to simplify the measurement of their polarization properties.

Figure 6 is a scanning electron micrograph of a photoresist grating fabricated in our laboratory. To fabricate this and other gratings, Shipley 1805 series positive photoresist was diluted to give nominal film thicknesses of 0.25 μm after spinning at 4000 rpm on soda-lime glass substrates. Gratings were then holographically generated in the photoresist layer using the Fresnel mirror method of Malag[15] at a wavelength of 0.4579 μm. The period of the gratings was chosen to be 0.24 μm to suppress all diffracted orders other than the 0th reflected. The gratings were monitored during development using a technique reported by Li et. al.[16] to ensure development to the substrate.

Following postdevelopment baking, 0.2 μm of silver was sputtered onto the photoresist gratings. Silver was used for the metallic coating because it is a better reflector than gold at λ=0.6328 μm. The refractive

indices of the substrate and silver were measured with a Gaertner L116C ellipsometer. The substrate refractive index was found to agree with the manufacturer's specification of 1.517. The real and imaginary parts of the silver refractive index were measured to be $n=0.12 \pm 0.02$, and $\kappa=2.48 \pm 0.01$. Measurement of the Fresnel reflection coefficient for incidence on the silver from the glass substrate confirmed the validity of these measurements. The period of this grating was measured optically to be 0.241 ± 0.001 μm, and the depth and duty cycle were estimated from the micrograph to be 0.28 ± 0.02 μm and 0.65 ± 0.05 respectively. The polarization state of a beam specularly reflected from the grating in Figure 6 was measured using the ellipsometer. A 45-45-90 prism was index matched to the back surface of the substrate to simulate substrate-mode incidence on the grating at 45°.

Figures 7a and 7b show experimental and calculated results for a polarization rotation grating (Element 3). Figure 7a is a plot of measured output polarization rotation angle (α_t) versus azimuthal angle Φ for p polarized light incident on the grating ($\alpha_i=0°$, $\delta_i=0°$). Note that at an azimuthal angle of incidence of -55°, this grating gives the desired output polarization angle of 45°. Plotted along with the experimental data are calculated results for reflection from a lamellar photoresist grating coated with silver with dc=0.65, $\Lambda=0.241$, d=0.24, $n_{photoresist}=1.64$, and the substrate and silver indices as above. The discrepancies between the curves can be attributed to the poor approximation of the actual grating profile by a lamellar profile.

Figure 7b shows measured and calculated diffraction efficiencies for this grating. The efficiencies are low (~0.5) because of the small value of the imaginary part of the silver refractive index. This value is dependent upon the method of deposition, which was sputtering for this element. Typical values for evaporated silver are near 4.0, which would increase the element efficiency.

5. OPERATIONAL TOLERANCES FOR GRATING ELEMENTS

The theoretical analyses of Section 3 indicate that it is possible to design the gratings required for the proposed detection train device. However, the impact of wavelength and incident phase difference variations on the performance of the elements must be evaluated.

The wavelength of laser diodes produced for use in M-O heads varies due to manufacturing tolerances. A realistic estimate of this variation is ±0.01 μm about the design value, which is 0.780 μm for the device we have modeled. This wavelength variation directly impacts the performance of Elements 1-4. Additionally, the propagation angle within the substrate in our proposed device is wavelength dependent due to the incoupling volume grating. For a beam normally incident on the incoupling grating, the propagation angle of the substrate-mode beam is given by

$$\Theta=\text{asin}(\lambda/n\Lambda). \quad (7)$$

Substituting the period of this grating (0.732 μm), the substrate refractive index (n=1.517), and the range of the wavelength variation (0.77 μm to 0.79 μm) into this equation gives the range of propagation angles within the substrate for which the elements must perform.

We investigated the influence of wavelength variation (with associated angle of incident variation) on the throughput efficiency of this device, the polarization state incident on Element 4, and the extinction ratios for the beams transmitted by Element 4. Figure 8 is a plot of system throughput efficiency for $\alpha_i=\pm 0.5°$ and $\delta_i=0°$ as a function of wavelength. The 1st order efficiency in this plot corresponds to the s polarized beam diffracted by the PBS for focus error sensing. The 0th order efficiency corresponds to the p

polarized beam used for tracking error sensing. An efficiency of greater than 0.69 for p polarization and 0.66 for s polarization is maintained over a wavelength range of 0.780 ± 0.01 μm.

Figure 9 is a plot of the rotation angle α_r of the beam incident on Element 4 as a function of wavelength for system input angles of $\alpha_i=\pm 0.5°$. Note that while the values of α_r for both incident rotation angles vary with wavelength, the separation between the two remains constant. Thus, minimal signal degradation occurs. The phase of this beam is not plotted because it is nearly invariant to wavelength variations.

Figure 10 is a plot of the extinction ratio of the s polarized 1st order and the p polarized 0th order diffracted by Element 4 (for the design of Section 3.4) as a function of wavelength. For this design, the extinction ratio of the s polarized 1st order is degraded with wavelength variation. However, the minimum extinction ratio of 31 still allows for differential signal generation.

An additional factor that influences the performance of the rotation grating (Element 3) is deviation of the incident state of polarization from left circular. As δ_i deviates from -90°, the magnitude of the Kerr rotation component is decreased after rotation (e.g. $\alpha_i=\pm 0.5°$ may be mapped to $\alpha_r=45.0 \pm 0.4°$ by reflection from the rotation grating). This is very undesirable, as this is a direct reduction of the signal. Figure 11 is a plot of rotation angle α_r versus δ_i for the design of section 3 with $\alpha_i=0.5°$. A typical range of δ_i for the incident beam is ±30° due to varying media ellipticities, M-O disk substrate birefringences, and phase differences introduced by the turning mirror and leaky beamsplitter. This figure shows that the maximum signal degradation is 20% over this range of δ_i.

6. CONCLUSION

In this paper, we have presented a novel device for providing M-O signal generation and error signal generation in a compact package. We also have presented gratings as polarization components in the M-O head detection train. We have experimentally demonstrated the polarization properties of one of the elements composing our proposed detection train device. This work suggests that significant miniaturization of the detection train can be accomplished if a minor decrease in detection train performance can be tolerated.

7. ACKNOWLEDGEMENTS

The authors gratefully acknowledge the assistance of L. Li of the Optical Data Storage Center, University of Arizona in modeling the polarization properties of surface-relief gratings. The authors acknowledge numerous helpful discussions regarding grating fabrication with L. Li, K. Bates, and K. Erwin, all of the Optical Data Storage Center, University of Arizona. The authors wish to acknowledge support for this work from IBM SUR-0499, a Litton ITEK Optical Systems Graduate Research Fellowship, and the Optical Data Storage Center of the University of Arizona.

* Current address: Consumer Electronics Laboratory, Mitsubishi Electric Corporation, 1 Zusho-Baba, Nagaokakyo-City, Kyoto 617, Japan

8. REFERENCES

1. Y. Ono, "Polarizing holographic optical elements for optical data storage," SPIE 1545, in press.
2. Y. Ono, "Holographic optical elements for optical disk R/W heads," Digest from Optical Memory Symposium '90 (in Japanese), July 1990, Makuhari, Japan.
3. S. Aoyama and T. Yamashita, "Grating beam splitting polarizer using multi-layer resist method," SPIE 1545, in press.
4. H. Maeda et. al., "A high density dual type grating for magneto-optical disk head," Japanese Journal of Applied Physics 28, Supplement 28-3, 193-195 (1989).
5. M. C. Gupta and S. T. Peng, "Multifunction grating for signal detection of optical disk," in Optical Data Storage, 1991, Technical Digest Series, 5 (Optical Society of America, Washington, DC 1988), 164-168.
6. T. D. Milster, "Characteristics of phase compensation techniques in magneto-optical read-back systems," SPIE 1166, 355-364 (1989).
7. N. Matsubayashi et. al., "Magneto-optical readout system by detecting elliptically polarized light," Proceedings of the Japan Society of Applied Physics Autumn Conference, 30A-PB-10 (1989).
8. C. W. Haggans and R. K. Kostuk, "Use of rigorous vector coupled-wave theory for designing and tolerancing surface-relief diffractive components for magneto-optical heads," SPIE 1499, 293-302 (1991).
9. M. G. Moharam and T. K. Gaylord, "Three-dimensional vector coupled-wave analysis of planar-grating diffraction," J. Opt. Soc. Am. 73, 1105-1112 (1983).
10. L. Li, "A modal analysis of lamellar diffraction gratings in conical mountings," to be submitted to J. Mod. Optics.
11. L. Li and C. W. Haggans, "On the convergence of the coupled-wave approach for lamellar diffraction gratings," accepted for Topical Meeting on Diffractive Optics, New Orleans, April 1992.
12. M. Born and E. Wolf, Principles of Optics (Pergamon, 6th ed. 1980), 24-30.
13. Interpolation of values from D. W. Lynch and W. R. Hunter, "Optical Constants of Metals" in Handbook of Optical Constants of Solids, E. D. Palik, ed., (Academic Press, 1985), Table II, 294.
14. C. W. Haggans, L. Li, T. Fujita, and R. K. Kostuk, "Modeling of lamellar phase retardation and polarization rotation gratings for substrate-mode devices," submitted to J. Opt. Soc. Am. A.
15. A. Malag, "Simple interference method of diffraction grating generation for integrated optics by use of a fresnel mirror," Opt. Commun. 32, 54 (1980).
16. L. Li, M. Xu, G. I. Stegeman, and C. T. Seaton, "Fabrication of photoresist masks for submicrometer surface-relief gratings," SPIE 835, 72-81.

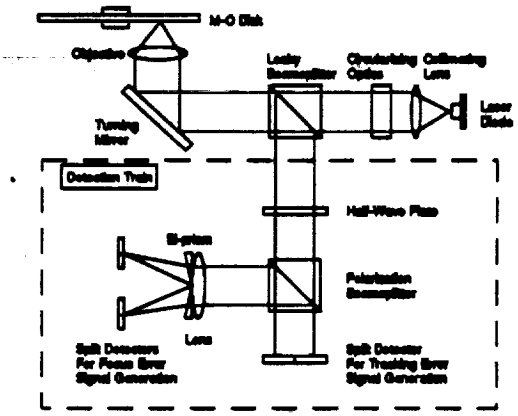

Fig. 1. Conventional M-O disk head layout.

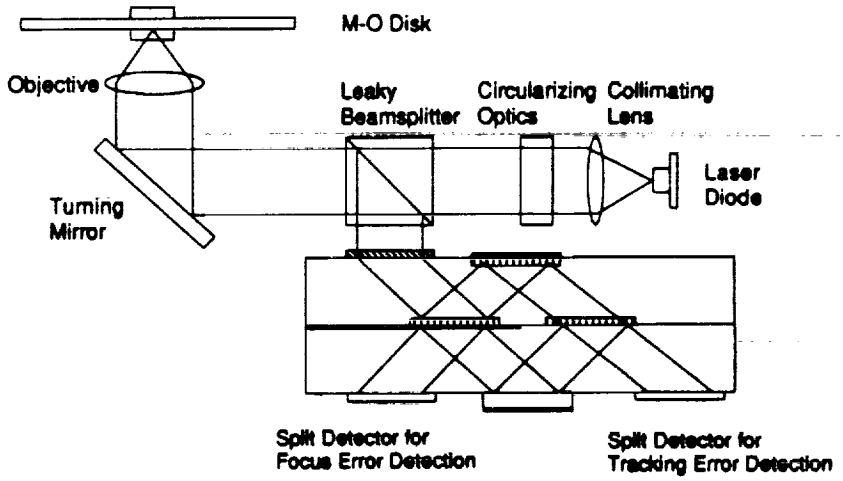

Fig. 2. Proposed M-O head with integrated detection train device.

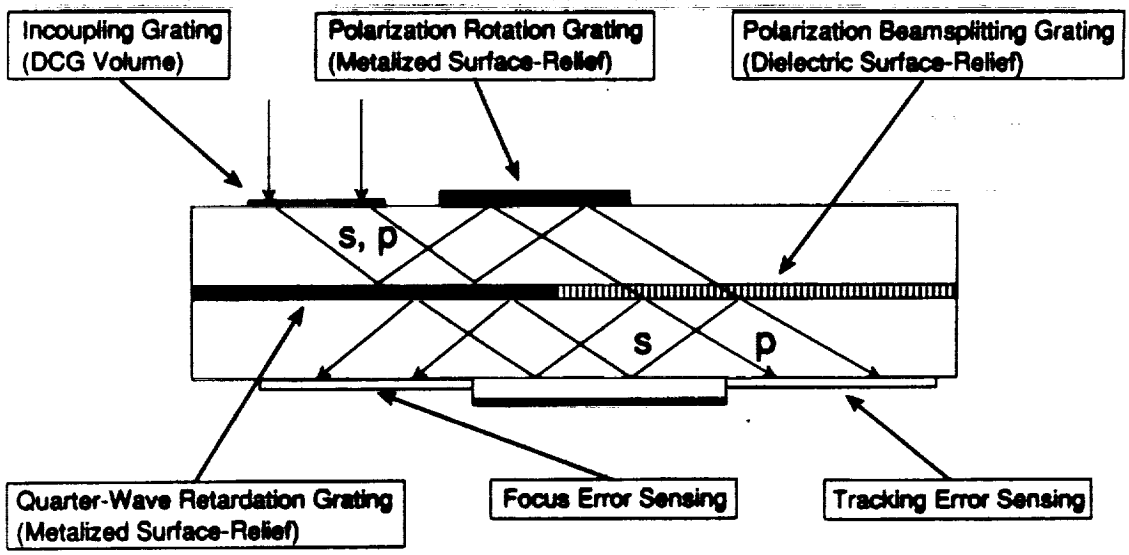

Fig. 3. Proposed detection train device.

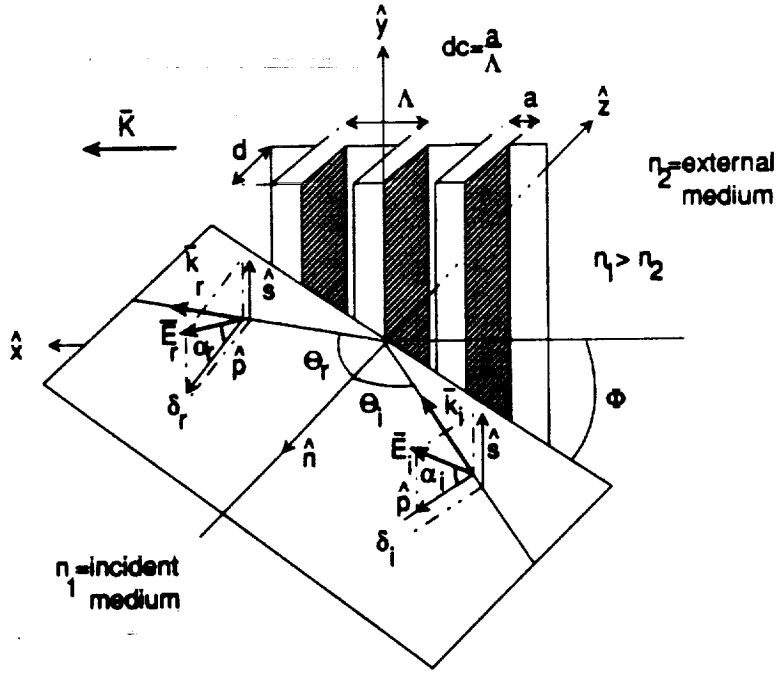

Fig. 4. Grating and incidence geometry.

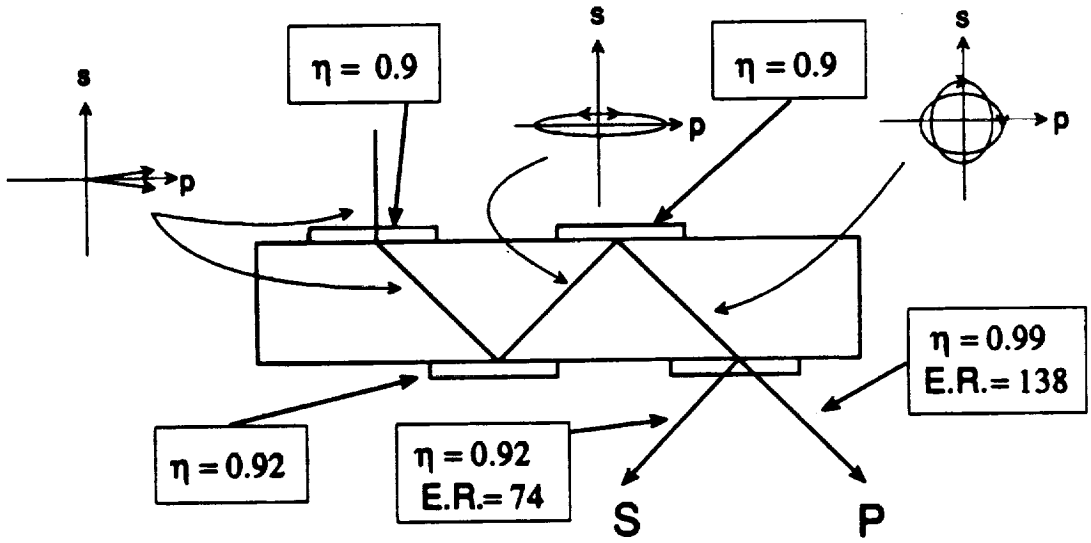

Fig. 5. Modeled device performance. The boxed quantities are individual element efficiencies. The polarization plots show the state of polarization at each point in the device.

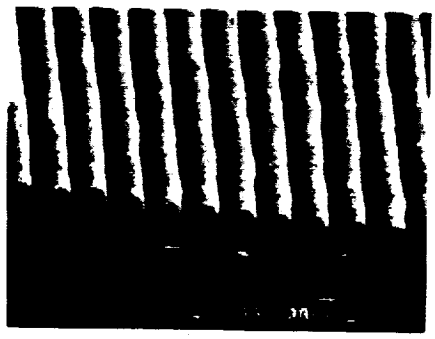

Fig. 6. Scanning Electron Micrograph of a photoresist grating fabricated in our laboratory.

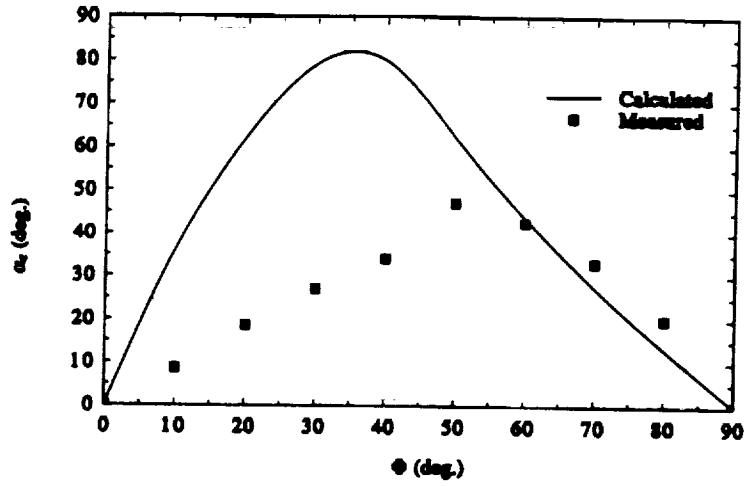

Fig. 7a. Measured and calculated values of the polarization rotation angle after reflection from the grating of Figure 6 (α_i=0°) as a function of the azimuthal angle of incidence.

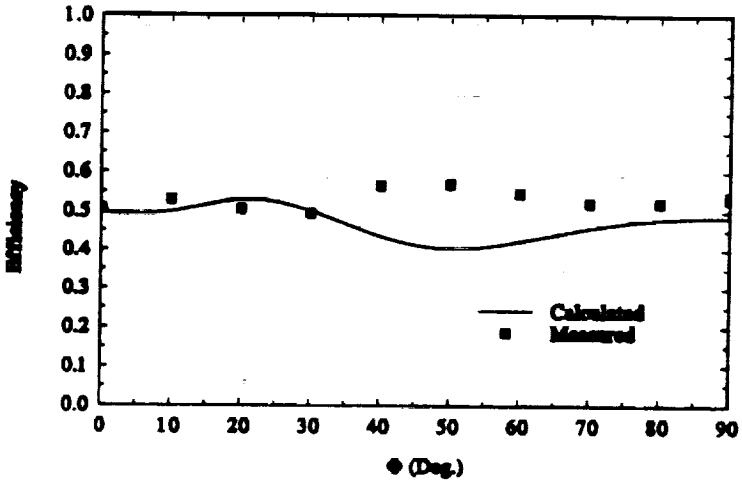

Fig. 7b. Measured and calculated values of the 0th reflected order diffraction efficiency as a function of azimuthal angle of incidence on the grating of Figure 6 .

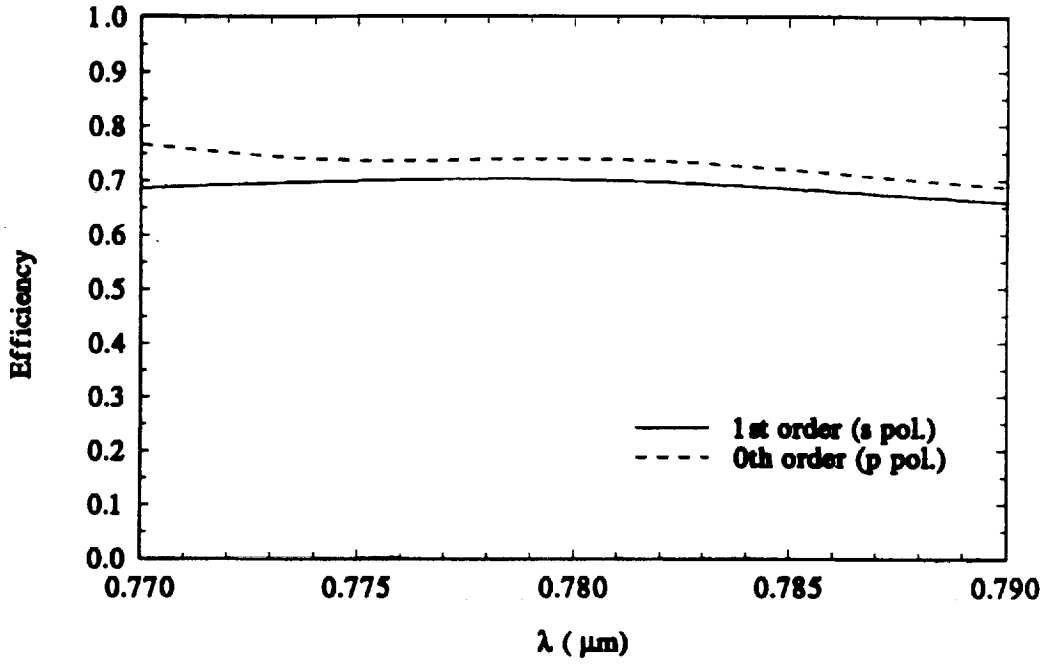

Fig. 8. Throughput efficiency for the device of Fig. 5 as a function of wavelength.

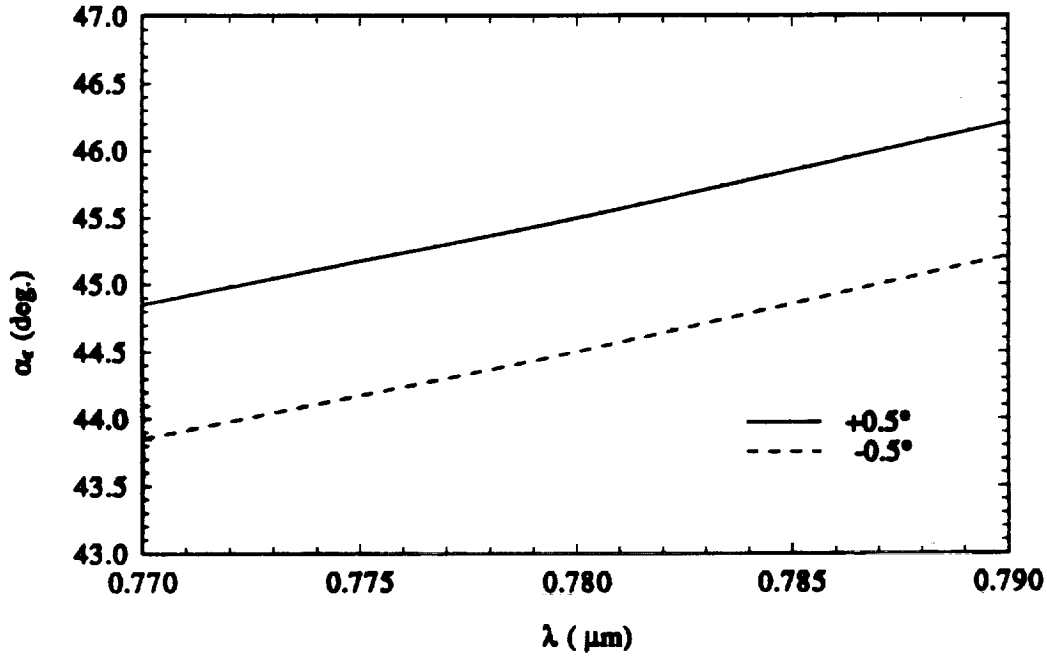

Fig. 9. Polarization rotation angle after Element 3 as a function of wavelength.

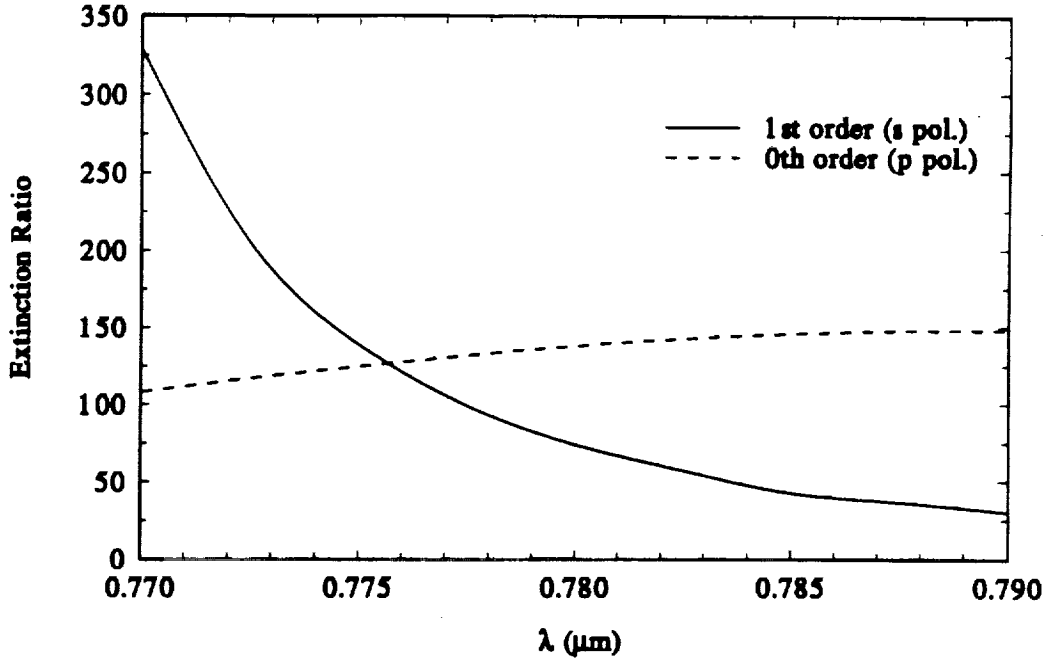

Fig. 10. Extinction ratio for Element 4 as a function of wavelength.

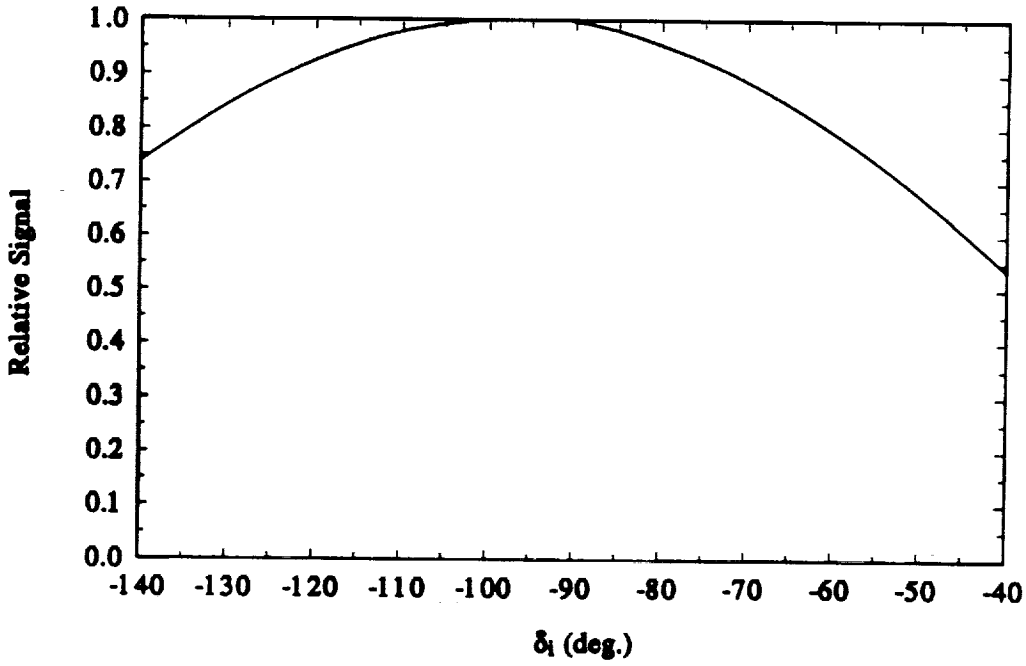

Fig. 11. Fraction of the ±0.5° input polarization rotation angle (input signal) remaining after Element 3 as a function of the phase difference incident on Element 1.

C-3

APPENDIX M